THERMAL IMAGE ANALYSIS FOR FAULT DETECTION AND DIAGNOSIS OF PV SYSTEMS

by

Hyewon Jeon

A Thesis

Submitted to the Faculty of Purdue University

In Partial Fulfillment of the Requirements for the Degree of

Master of Science

Department of Computer and Information Technology

West Lafayette, Indiana

May 2020

THE PURDUE UNIVERSITY GRADUATE SCHOOL

STATEMENT OF COMMITTEE APPROVAL

Dr. John A. Springer, Chair

Department of Computer and Information Technology

Dr. Byung-Cheol Min

Department of Computer and Information Technology

Dr. Dawn Laux

Department of Computer and Information Technology

Approved by:

Dr. Eric T. Matson

Head of the Graduate Program

ACKNOWLEDGMENTS

This thesis is dedicated to my dear parents for their unwavering support and sacrifice for my education.

I also acknowledge Dr. John A. Springer, Dr. Byung-Cheol Min, and Dr. Dawn Laux for their guidance and encouragement.

Last but not least, I would like to thank my dear friends, who have always been there for me.

TABLE OF CONTENTS

LIST OF TABLES

LIST OF FIGURES

LIST OF ABBREVIATIONS

AH	Ampere Hour
DA	Data Acquisition
DD	Decimal Degrees
FDD	Fault Detection and Diagnosis
GPS	Global Positioning System
HS	Hot Spot
IR	Infrared
IRT	Infrared Thermography
IV	Current–Voltage
LWIR	Long Wave Infrared
O&M	Operations and Maintenance
PV	Photovoltaic
PVM	Photovoltaic Module
PVS	Photovoltaic System
RGB	Red, Green, and Blue
STM	Science, Technology, and Medicine
UAV	Unmanned Aerial Vehicle

GLOSSARY

Hot Spot: “Hot spot heating occurs in a PV module when its operating current exceeds the reduced short-circuit current (Isc) of a shadowed or faulty cell or group of cells. When such a condition occurs, the affected cell or group of cells is forced into reverse bias and dissipates power, which can cause local overheating” (Deng and Xing, 2017, p. 80).

Aerial Thermography: “Aerial thermography is a remote sensing technique that displays the apparent temperatures of objects in a scene” (Allinson, 2007, p. 2).

IR Thermography: “Infrared thermography is the science of detecting infrared energy emitted from an object, converting it to apparent temperature, and displaying the result as an infrared image” (Fluke, n.d., para. 2).

Thermal Anomaly: “Thermal Anomaly means a departure from a reference value or long-term average. A positive anomaly indicates that the observed temperature was warmer than the reference value, while a negative anomaly indicates that the observed temperature was cooler than the reference value” (Portland Cement Association, n.d., para. 1).

ABSTRACT

Author: Jeon, Hyewon
Institution: Purdue University
Degree Enrolled: August 2018
Title: Thermal Image Analysis for Fault Detection and Diagnosis of PV Systems
Major Professor: John A. Springer

This research presents thermal image analysis for Fault Detection and Diagnosis (FDD) of Photovoltaic (PV) Systems. The traditional manual approach of PV inspection is generally more time-consuming, more dangerous, and less accurate than the modern approach of PV inspection using Aerial Thermography (AT). Thermal image analysis conducted in this research will contribute to utilizing thermography and UAVs for PV inspection by providing a more accurate and cost-efficient diagnosis of PV faults. In this research, PV module inspection was achieved through two steps: (i) PV monitoring and (ii) PV Fault Detection and Diagnosis (FDD). In the PV monitoring stage, PV cells were monitored by aerial thermography. In this stage, the thermal data was acquired for the next step. In the PV FDD stage, hot spot phenomenon and the condition of the PV modules were detected and measured. The FDD stage was conducted in three steps: (i) fault detection, (ii) fault isolation, and (iii) fault identification. The fault detection stage determined whether the PV module has an abnormal condition. Next, in the fault isolation stage, the location and the area of possible hot spots were identified. Lastly, the number of the hot spots were counted in the fault identification stage. The proposed research will help with the problems of the modern PV inspection and, eventually, contribute to the performance of PV power generation.

CHAPTER 1. INTRODUCTION

Photovoltaic (PV) systems, also known as solar panels, are gaining more attention nowadays than ever. The global PV market has grown exponentially from 1992 to 2019, and the market is expected to grow faster in the coming years (Willoughby, 2019). According to a market report, Renewables 2019 by IEA (n.d.), the maximum amount of energy produced by renewable energy is estimated to increase by 50% between 2019 and 2024. The IEA addresses that Solar PV accounts for about 60% of the increase.

Although the worldwide PV market has been growing, most of the Operations and Maintenance (O&M) work is being handled bytraditional manual methods. These methods require a considerable amount of human labor, and sometimes it is dangerous. Please see Willoughby (2019) for the traditional and the modern methods of PV inspection. United States Department of Labor addressed, "workers in the solar energy industry are potentially exposed to a variety of serious hazards, such as arc flashes (which include arc flash burn and blast hazards), electric shock, falls, and thermal burn hazards that can cause injury and death" (United States Department of Labor, n.d., para. 5). There is a need to build a solution that provides economical operation and safe maintenance.

Utilizing Aerial Thermography (AT) with Unmanned Aerial Vehicles (UAVs) has become an emerging solution for a PV system inspection. UAVs can collect data more than 50 times faster than traditional handheld methods by flying over PV modules and also guaranteeing safety by avoiding dangerous working conditions. Additionally, PV inspection using UAVs promotes accuracy in data management and data integrity (Willoughby, 2019). AT for PV inspection allows us to "assess performance of photovoltaic modules, superseding time-consuming traditional manual methods" (Gallardo-Saavedra, Hernández-Callejo, and Duque-Perez, 2018, p. 1).

This chapter introduces an overall introduction to the research subject. It includes the problem, significance, the purpose, research questions, assumptions, delimitations, and limitations.

1.1 The Problem

At present, most of the PV system inspections are operated by traditional manual methods, which are inefficient, inaccurate, and hazardous. This is why the new application of aerial thermography with UAVs has become a new solution for the inspection of PV systems. Aerial thermography with UAVs provides a reliable and high-performing method for a PV system inspection. However, there exists a limitation of using thermography occurring from irradiance and the environmental condition.

1.2 Significance

With worldwide PV market growth and support from the government, the demand for PV system installation and O&M is rising. Moreover, solar panels can be pricey. “Solar panel costs for an average-sized installation in the U.S. usually range from $10,836 to $14,196 after solar tax credits” (MATASCI, 2019, para. 4). Considering the initial cost of operating PV systems, it is economical to keep them longer. Effective and timely inspections are a necessary part of O&M for ensuring durable PV systems. Especially, PV systems require regular inspections, not like other artificial infrastructure objects (UgCS, n.d.). A PV cell, a basic unit of PV systems, has the potential to affect the performance of the entire system. Any internal or external defects can drastically decrease the whole power generation performance of the PV module (Lee & Park, 2019).

PV systems are installed in varied scales. In most cases, PV systems are mounted on roofs to generate electricity for residential energy needs. When the PV systems become massive, they are called PV power stations, also known as solar parks, solar farms, or solar ranches. Energy generated by PV solar farms is transmitted through the electric grid and powers thousands of houses, businesses, and even cities (Renewable Energy World, 2019). Regarding the various application of PV systems and their sizes, inspecting them in a handheld way is very inefficient and dangerous.

The PV module inspection system suggested in this study is significant because it enables safe condition monitoring and accurate Fault Detection and Diagnosis (FDD). The proposed system uses UAVs and thermal cameras to maximize the efficiency of fault detection of PV systems. UgCS addressed that a "drone equipped with thermal camera is the best choice for solar panel field inspection, as in most cases it saves costs compared to manned aviation and saves time compared to visual control with handheld IR camera" (UgCS, n.d., para. 2). In addition, the research uses an image analysis technique to analyze the condition of PV modules accurately. To summarize, the proposed system will eventually minimize harms and enhance the accuracy of PV inspection by applying reliable and efficient methods.

1.3 The Purpose

The purpose of the study is to detect the hot spot phenomenon on PV modules using aerial thermography. Specifically, the study focuses on analyzing the differences in the thermal appearances of PV faults in different PV conditions, to provide meaningful factors for the modern PV inspection approaches.

1.4 Research Questions

- How effective is it to utilize aerial thermography for PV module inspection?
- What are the differences in the thermal appearances of the PV faults in different PV conditions?

1.5 Assumptions

- PV modules generate electrical energy in real-time.
- The AT method used in this study can realize a close-range UAV flying.

1.6 Delimitations

- Out of many kinds of PV module faults, the study focuses on the Hot Spot (HS) phenomenon.
- One mono crystalline PV module was subjected to inspection.
- The PV module has outer dimensions of 24.84 x 21.81 inches and consists of 36 individual cells that measure 5 x 2.55 inches each.
- One type of PV modules was inspected in the experiments.
- One type of UAVs, *PHANTOM 2 (n.d.)*, was used for a close-range UAV realization.
- One type of thermal sensors, *Seek Thermal Compact (n.d.) for Android*, was used to collect thermal images.
- Seek Thermal Compact has a resolution of 206x156 pixels with a 36° field of view.

1.7 Limitations

The limitations of the research include:

- The experiment was conducted in a location with the GPS coordinates of 40.425965, -86.909730 (DD).
- The experiment was conducted on November 26, 2019.
- The performance of PV modules was easily affected as the weather changes.
- The amount of sunlight was not constant.

1.8 Summary

This chapter provided the purpose and the problem of the study. Specifically, it covers the introduction, the problem, the significance, the purpose, the research questions, the assumptions, the delimitations, and the limitations of the research.

CHAPTER 2. LITERATURE REVIEW

2.1 Methodology of the Review

The diversity of the research subject 'Thermal Image Analysis for Fault Detection and Diagnosis of PV Systems' can be classified into three fields: (i) PV systems inspection, (ii) Aerial Thermography (AT), and (iii) Fault Detection. The literature review process consists of searching four scientific search engines, *IEEE Xplore digital library*, *Springer*, *ScienceDirect*, and *Google Scholar*. These scholarly resources are known for the most promising databases in science and engineering fields.

The literature review was initiated by reviewing the recent research trends in the relevant fields of the research. *ScienceDirect (n.d.)* and *Google Scholar (n.d.)* were used for the initial search step. After examining the initial group of scientific resources, the author moved on to searching for studies more relevant to the study. In this step, most of the references were found in *IEEE Xplore digital library* published by the Institute of Electrical and Electronics Engineers (IEEE) (IEEE Xplore® Digital Library, n.d.). Additionally, *Springer* was used to finding suitable literature. After evaluating the second group of articles from *IEEE Xplore® Digital Library (n.d.)* and *Springer (n.d.)*, some of them were discarded from the references for this study. In addition, the author manually reviewed the related publications including *Energies*, *Renewable and Sustainable Energy Reviews*, and *Solar Energy*.

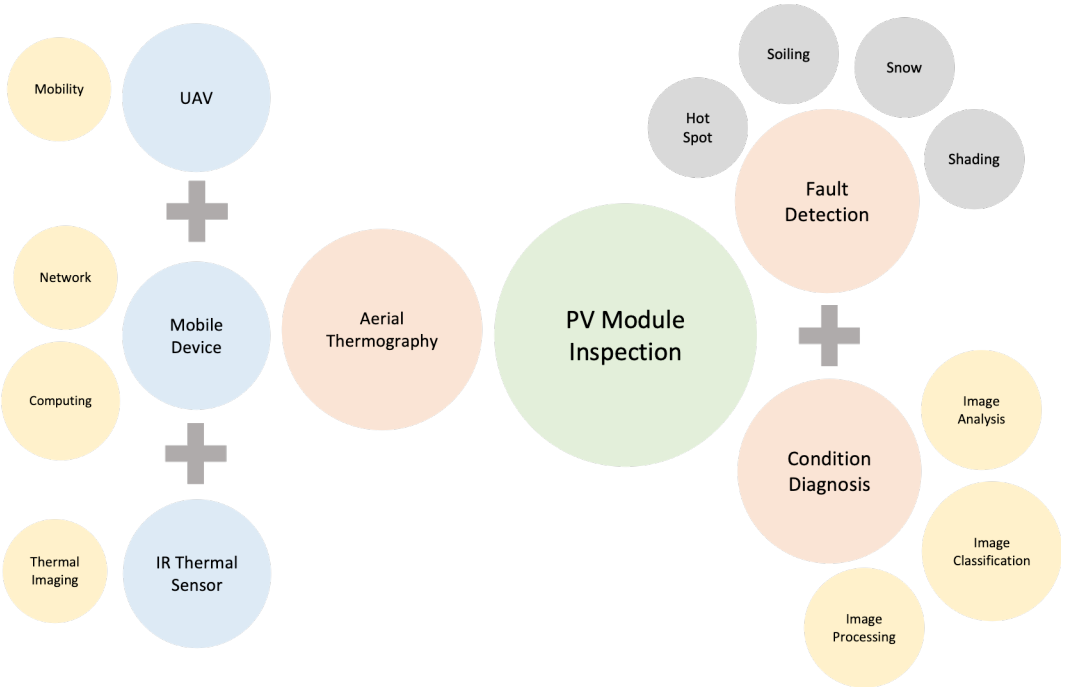

Figure 2.1. Key concepts in the concept map

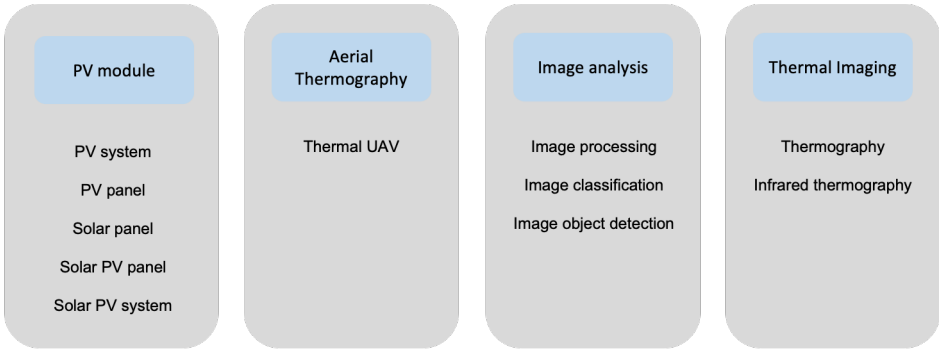

Figure 2.2. Key concepts that were used synonymously

Key concepts of the literature study involve PV module inspection, aerial thermography, fault detection, and others. The key concepts are present in the concept map in *Figure 2.1.* The author used *PV module*, *PV panel*, *PV system*, *solar panel*, *solar PV panel*, and *solar photovoltaic system* synonymously when doing literature searching. The key concepts and their synonyms are listed in *Figure 2.2*. The author used the overlapping areas of the three main key concepts, PV module inspection, aerial thermography, and fault detection, for the search input in order to find relevant literature. The Venn diagram shown in *Figure 2.3* shows the search strategy of the literature study.

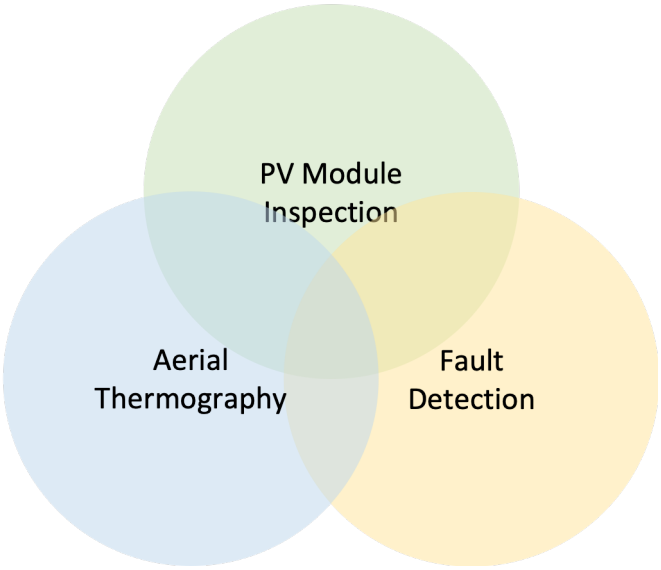

Figure 2.3. Search strategy in Venn diagram

2.2 Findings Pertaining to the Problem & Purpose

The world uses 35 billion barrels of oil every year (Jean-Paul & Claude, 2017). This huge dependence on fossil fuels pollutes the Earth and oil is not a permanent energy source. According to the U.S. Energy Information Administration (2019), the U.S. consumed about 20.5 million barrels of petroleum per day in 2018. If this trend continues, oil and gas in the Earth will be depleted in 53.3 years (George, 2014). On the other hand, we have rich energy sources on the planet Earth, such as sun, wind, water, and geothermal energy. The energy generated by these sources is called renewable energy, sustainable energy, or alternative energy. These energy sources could replace traditional energy sources such as oil and coal (SunPower, n.d.).

Governments and businesses have tried to popularize renewable energy for decades with the hope of harnessing natural energy sources to meet our complete needs in energy. However, renewable energy is expected to fulfill only up to 13% of our needs as of 2020 (Hodge, 2019). Although satisfying the full need for energy with renewables looks challenging now, on the bright side, our technology is highly advanced enough to utilize renewables, and there is an abundant supply of renewable energy. The Earth intercepts 50 quadrillion watts of solar energy per day (Farret & Simões, 2017). That amount is more than enough to support the entire civilization (Farret & Simões, 2017).

Someone might wonder why we do not solely depend on solar energy. That is because there are hurdles to overcome. Operations and Maintenance (O&M) for alternative energy is still expensive and not easily accessible (Ellsmoor, 2019). Therefore, “at present, the greatest advances in photovoltaic systems (regardless of the efficiency of different technologies) are focused on improved designs of photovoltaic systems, as well as optimal operation and maintenance” (Hernández-Callejo, Gallardo-Saavedra, and Alonso-Gómez, 2019, p. 1). There is a need to develop an innovative and efficient PV system inspection.

2.3 Findings Pertaining to the Methodology of Cited

2.3.1 Motivation

The motivation of this research is to continue the author's previous research, "Analyzing the Range of Angles of a Solar Panel to Detect Defective Cells, using a UAV" (Kim et al., 2019, p. 471). The precedent research was conducted during the fall of 2018 at Purdue University and was published at *5th Workshop on Collaboration of Humans, Agents, Robots, Machines and Sensors (CHARMS 2019)* in Naples, Italy. The research received positive reviews and was identified as one of the best papers accepted for the conference.

The paper focuses on improving the power generation efficiency of solar panels. The study designed and implemented a thermal UAV system that analyzes "the range of angle between a solar panel and thermal camera to detect defective cells of the solar panel effectively" (Kim et al., 2019, p. 471). The study also "developed an algorithm that detects defective solar cells using computer vision" (Kim et al., 2019, p. 471). In conclusion, the research identified "the relationship between the angle of the solar panel and the detection of the defective cells" (Kim et al., 2019, p. 475).

2.3.2 Photovoltaic (PV) Technologies Overview

Photovoltaic is a carbon-free technology that converts sunlight into a form of electrical energy (Lynn, 2011). A PV Cell or a Solar Cell is a semiconductor device. There are multiple different types of solar cells of which three most common technologies are monocrystalline, polycrystalline and amorphous silicon solar cells (Fraunhofer Institute for Solar Energy Systems, 2019). Monocrystalline silicon solar cells are a high-performance solar technology that typically has higher efficiency, but also higher cost when compared to other technologies. Polycrystalline silicon solar cells are less efficient than monocrystalline solar cells but cost comparatively less. Amorphous silicon solar cells are even less efficient than polycrystalline solar cells but are still lower cost (Parida, Iniyan, & Goic, 2011). Polycrystalline solar cells have a leading market share amongst silicon based solar panel technologies although monocrystalline cells have recently gained some market share (Fraunhofer Institute for Solar Energy Systems, 2019). Multiple individual PV cells are interconnected to form a PV Module or a PV Panel to increase PV utility. PV modules can form a PV Array when they are wired in a row. These different types of PV systems are shown in *Figure 2.4.*

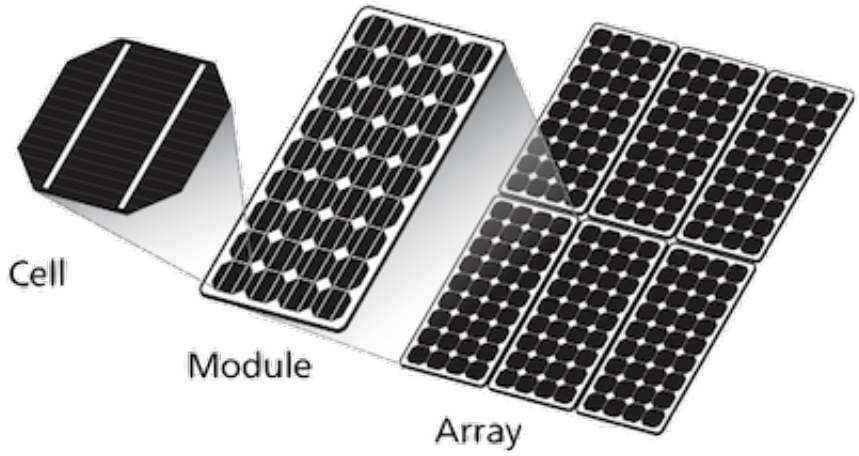

Figure 2.4. PV Cell, Module, and Array. Retrieved from "Solar (PV) Cell Module, Array", by Samlex America Inc (n.d.).

PV systems come in diverse scales and shapes. When PV systems become utility-scale, the energy generated by them can support millions of people, thousands of houses, and communities (Becker, 2019a). These large-scale PV systems are called PV power plants or solar farms. *Solar Star* built in June 2015 is the largest PV power plant in the U.S. "It consists of 1.7 million solar panels spread out over 13 square kilometers (or 3,200 acres) in Kern and Los Angeles Counties, California" (Becker, 2019b, para. 3). It produces 579 megawatts of energy, which is enough electricity to power about 255,000 households in California.

2.3.3 Hot Spot Phenomenon in PV Systems

Identifying defects in PV modules is crucial because these faults can prompt severe power losses and degenerate performance. A single fault in a cell has the potential to spread to other modules near it and result in a complete failure in its functioning (Mapundu, 2018). There are three types of PV system faults: (i) module faults, (ii) string and system faults, and (iii) racking and balance of the system. For the module faults, there are "hot spots on the cells, diode failure, shattered or dirty modules, coating and fogging issues, and junction box heating" (Constantin and Dinculescu, 2019, p. 3). For the string and systems faults, there are "wiring issues (reversed polarity, frayed cables), charge controller issues, and inverter and fuse failures" (Constantin and Dinculescu, 2019, p. 3). Out of these varied PV faults, this research focuses on Hot Spot (HS) phenomenon, which is the primary defect of PV modules. Therefore, HS has been a popular research topic in the photovoltaic systems field (Lee & Park, 2019).

HS is a phenomenon in PV modules when a cell in a PV panel acts as a load for other cells and significantly harms the substantial performance of itself and the cells linked to itself (Lynn, 2011). This phenomenon is a sign of energy loss in PV modules and it is considered as one of the critical faults in PV modules. The leading causes of the hot spots are PV cell failures, partial shadowing, PV cell mismatch, or connection failures in cell links (Molenbroek, Waddington, & Emery, 1991).

2.3.4 Cell Mismatch in PV systems

The leading cause that facilitates hot spot phenomenon is cell mismatch. It occurs "when cells of varying current are connected in series which can often be mitigated via the solar panels bypass diodes" (Solar Review, 2018, para. 6). When it happens, the amount of energy generated by the modules is limited by the cell with the lowest performance, which results in energy loss. When utilizing PV modules, it is challenging to avoid small-scale manufacturing tolerance, minor cracks, meager temperature differences depending on the locations of the PV module and partial shades in the PM module (Lynn, 2011). Partial shading, soiling, or aging in photovoltaic modules result in a serious energy loss in PV performance (Olalla, Hasan, Deline, & Maksimović, 2018).

2.3.5 Shadow Effect on PV Systems

Shadow Effect on PV systems is a common but critical problem. According to Deutsche Gesellschaft für Sonnenenergie (DGS), "in a large number of these systems, shading caused annual yield reductions of between 5 percent and 10 percent. Shading can be classified as temporary, resulting from the location, the building, or caused by the system itself (self-shading)" (Deutsche Gesellschaft für Sonnenenergie (DGS), 2013, p. 173). Shadow effect on PV systems can be categorized into two groups, direct shadows and temporary shadows. In particular, direct shadows can result in a significant impact on the PV module. In the case of temporary shadows, circumstances like snow, leaves, animal droppings, and other objects on PV modules can result in a shading effect (Deutsche Gesellschaft für Sonnenenergie (DGS), 2013). *Figure 2.5* shows an example of a shadow effect on PV modules.

Figure 2.5. Shading Effect on PV modules: No shading (left) and shading (right)

2.3.6 Soiling Effect on PV Modules

Soiling means an accumulation of dirt on PV module surfaces (Piliougine, Carretero, Sidrach-de Cardona, Montiel, & Sánchez-Friera, 2008). When it comes to soiling, the meaning of 'dirt' contains not only dust but also snow, leaves, pollen, animal droppings, and any other object stacked up on PV modules (Maghami et al., 2016). It is considered one of the significant causes of energy losses in PV systems performance. "Soiling is a complex problem that increases uncertainty and drives up the levelized cost of energy through lost energy production, increased operation and maintenance costs, and financing rates" (U.S. Department of Energy, 2018, p. 47). "Soil deposition can result into cementation, which eventually leads to an energy loss of up to 100%" (Fagnani, 2016, para. 5). *Figure 2.6* shows one example of soiling effect on PV modules.

Figure 2.6. Soiling effect

Due to its significance, recent studies have shown interest in the impact of soiling effect on PV modules. In recent years several studies have been conducted to estimate the impact of soiling on photovoltaic modules. According to Fagnani, the most influential factors that preceed soiling losses are "the dust properties (size, shape. . .), the chemical components in soil, pollution, moisture, rainfall frequency and intensity, wind speed, direction, and PV array structural configuration" (Fagnani, 2016, para. 4). Amongst the factors, tilt-angle (direction) and structural configuration of PV array are the most critical causes. An in-depth study conducted by Cano has proven that "the soiling effect is present at any tilt angle, but the magnitude is evident: the flatter the solar module is placed, the more energy it will lose" (Cano, 2011, p. 48). In 2016, Maghami et al. researched Power loss due to soiling on a solar panel. It addresses that "there are two types of soil shading on PV modules, which are known as hard shading and soft shading. Soft shading takes place when some materials such as smog are in the air, and hard shading occurs when a solid such as accumulated dust blocks the sunlight in a clear and definable shape" (Maghami et al., 2016, p. 1313).

2.3.7 Snow Effect on PV Modules

Soiling effect can pose serious harm in places where snow accumulates and remains for a long time. “Snow cover can be seen as a special case of soiling applicable in countries with colder climate” (Stridh, 2012, p. 1). In this condition, where snow entirely covers up PV modules, the performance of the PV modules can be badly decreased. An example of the snow effect on PV modules is present in *Figure 2.7.* It is recommended to arrange the PV modules horizontally than vertically to minimize the loss because electrical strings of vertically arranged PV modules will be more affected by the snow effect (Deutsche Gesellschaft für Sonnenenergie (DGS), 2013).

Figure 2.7. Snow effect

2.3.8 Fault Detection and Diagnosis (FDD) in PV systems

Fault Detection and Diagnosis (FDD) methodology can be achieved through the three main steps shown below.

1. Fault detection: “The indication that something is going wrong in the monitored system” (Gertler, 2017, p. 3).
2. Fault isolation: “The determination of the exact location of the fault” (Gertler, 2017, p. 3).
3. Fault identification: “The determination of the magnitude of the fault” (Gertler, 2017, p. 3). Step two (fault isolation) and three (fault identification) are the subsets of ‘Fault Diagnosis.’

Fault detection and diagnosis methods can be categorized into two main classes, (i) visual and thermal methods and (ii) electrical methods. Visual methods are suitable for "detecting discoloration, browning, surface soiling, hot spot, breaking, and delamination," and electrical methods are suitable for "detecting and diagnosing faulty PVM, strings, and arrays including arc fault, grounding fault, diodes fault, etc" (Mellit, Tina, and Kalogirou, 2018, p. 6).

Traditionally, the latter method, the electrical method, had been the most attracted for FDD. "Manual electrical testing is the de facto method of inspecting PV systems. Known as IV Curve Tracing, the test is the current industry standard for inspecting and evaluating performance of a solar array" (FLIR, 2019, p. 4). According to Piliougine, Carretero, Mora-López, and Sidrach-de Cardona, IV curve tracing works "based on the control of the voltage at module terminals between the short-circuit point and the open-circuit point" (Piliougine et al., 2011, p. 591). Undoubtedly, IV curve tracing has contributed significantly to PV system FDD. In spite of the benefits of applying IV curve tracing, it is not the most efficient and easy way to perform FDD. IV curve tracing method requires "trained, highly skilled technicians using handheld testing kits during only ideal environmental conditions such as dry, relatively-clear weather with little to no wind" (FLIR, 2019, p. 4). Additionally, PV modules must be set to a specific condition to test its performance, and the testing specialists have to check five symptoms of PV failures manually (FLIR, 2019). The electrical method also has limits in integrity in fault diagnosis. Gallardo-Saavedra et al. pointed out that "electrical tests allow detection of abnormal underperforming situations but do not recognize the cause or the location of the faulty module or cell" (Gallardo-Saavedra et al., 2018, p. 574).

This study adopted a method that is classified in the other method group, visual and thermal methods, with the application of UAV to overcome the weaknesses of the electrical method. This approach is also called Aerial Thermography (AT), which means "the use of drone thermal imaging for PV inspections" (FLIR, 2019, p. 5). While the manual electrical test for PV inspection takes many hours and days, PV inspection applying UAV thermal imaging can be done in a day. In the next paragraphs, the impact of using thermal imaging and UAV is explained.

Thermal imaging, also known as Infrared Thermography (IRT), is a powerful inspection tool to assess the performance of PV modules. It uses Long Wave Infrared (LWIR) cameras, also known as thermal cameras, to "detect the infrared band of the electromagnetic spectrum" (FLIR, 2019, p. 5). The main benefit of using a thermographic camera to monitor PV modules is safe and efficient while not interfering with the PV systems' operations (Glavaš, Vukobratović, Primorac, & Muštran, 2017).

Though IRT technology surpasses the electrical methods in terms of inspecting PV modules, on-site PV inspection using a hand-held thermal camera is still not sufficient. The application of UAV must be considered to design an optimal PV inspection methodology. Gallardo-Saavedra et al. addressed that "the application of UAVs in a thermographic inspection of photovoltaic modules is a major advancement in O&M activities of PV plants" (Gallardo-Saavedra et al., 2018, p. 574). With this regard, thermal UAV has become the mainstream methodology for PV inspection. Therefore, there are a number of studies on UAV thermal imaging for PV inspections (Constantin & Dinculescu, 2019). The research on aerial thermography for monitoring PV systems started in the early 21st century (Gallardo-Saavedra et al., 2018). In 2012, Denio (2012) used aerial solar thermography to monitor the condition of PV systems that are mounted on rooftops and in an extensive area. The study proved that aerial thermography is a reliable solution to detect faults in solar arrays, but the causes of the faults still needed to be confirmed. Later in 2015, Kauppinen et al. (2015) compared two PV solar plant measurement approaches using IR scanning, one from the ground and the other one using a UAV. The study concluded that the test of the IR measurement method using UAV was successful. In recent years, studies have shown their interests in computer vision approaches to automate Fault Detection (FD) (Gallardo-Saavedra et al., 2018). Jaffery, Dubey, Haque, et al. (2017) proposed the application of fuzzy logic and heuristic knowledge to fault classification and analysis respectively on thermal images of PV modules. Their method presented a reliable fault diagnosis. Real world experience of AT inspections of large PV installations in Turkey found the method to be the most efficient in finding faults. Hot spots made up 25% of all found faults in these inspections and the most common reason for the hot spots was soiling (Cubukcu & Akanalci, 2020).

2.3.9 Thermal camera considerations for PV module inspection

There are two general types of thermal cameras that are cooled and uncooled. Most small unmanned aircraft use uncooled sensors due to their lower prices and lower weight, which is essential for aircraft. Actively cooled thermal cameras are more sensitive to temperature differences, but there exist uncooled thermal cameras with acceptable sensitivity for aerial thermography of PV installations. Important properties to take into account when doing PV module aerial thermography include a field of view, sensor resolution, and camera distance from a PV module. To detect faults in an individual PV cell, the cell area in an image should be at least 3 to 5 times larger than an individual pixel. Thermal cameras can be radiometric, which means that each pixel has a temperature value. Without radiometric function, a thermal camera only shows the relative differences in temperature, but accurate measurement of temperature is not possible (Gallardo-Saavedra et al., 2018).

2.4 Summary

In this section, the methodology of the review, the findings pertaining to the problem and purpose, and the findings pertaining to the methodology of cited were reviewed. The precedent research was introduced in the motivation section, and the background knowledge of PV systems and PV failures were followed. In the last part, the findings about the proposed methodology were addressed. The approach of the research contains two steps, PV module monitoring and PV module FDD. PV monitoring using the suggested aerial thermography system, and the FDD methods are presented in the next chapters.

CHAPTER 3. METHODS

3.1 Introduction

The traditional PV system inspection is inefficient, inaccurate, and dangerous. Therefore, the new approach of PV system inspection using aerial thermography has become a solution in the industry. The thermal image analysis method introduced in this chapter will help PVS inspection by finding and analyzing the thermal appearances of PV faults and eventually provide meaningful factors for PV inspection using aerial thermography. The key strengths of these research methods are reliability and accuracy in hot spot detection. This research takes three main steps to conduct a PV module inspection: (i) Thermal data collection for PV module monitoring, (ii) Thermal image preprocessing, and (iii) Thermal image data analysis for PV fault detection and diagnosis (FDD). The research overview is present in the research overview in *Figure 3.1*. This chapter mainly focuses on the data preprocessing method and the data analysis method. The data collection experiment is explained in Chapter 4.

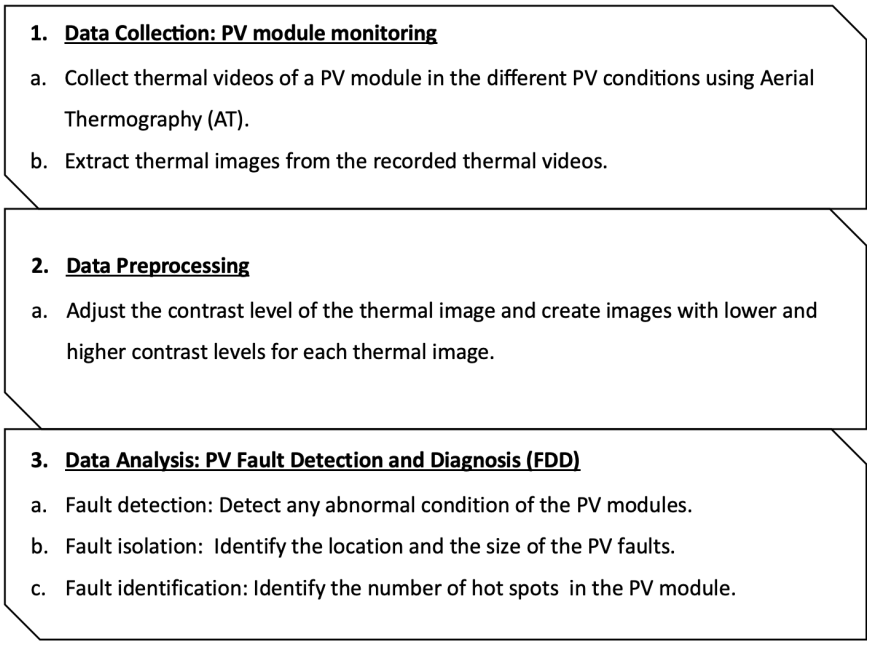

Figure 3.1. Research overview in steps

3.2 Thermal Image Data Preprocessing

Image preprocessing procedures can help to understand the error range of hot areas in thermal images, and enhances the characteristics of the data. Thermal cameras work as they calculate the relative temperature differences between the objects in the camera view. This results in images having an unstable presentation of the areas with the same temperature. Therefore, raw thermal images can have high noise in the data. This phenomenon can lead the faulty areas in the thermal presentation to have errors.

The image preprocessing method used in this research captured the accurate hot spot area regarding that hot spot area appearing in thermal images have errors, compared to the physical hot spot area in the PV module. The research originally tested a few different approaches to maximize the hot spot feature of the thermal data while capturing the faults correctly. This testing experiment was done through two steps. First, the image preprocessing operations listed below were initially applied to the thermal data collected. Each operation was tested individually and, also, multiple operations of them were tested jointly. This process was done to see what approach is the most effective to extract important features of the hot spot phenomenon. As a result of the first stage, adjusting the contrast level was shown to make meaningful changes in the thermal images. It was able to present reliable hot spot error ranges while not missing the hot spot features.

- Adjusting the contrast level.
- Adjusting the sharpness level.
- Adjusting the pixel brightness level.

The research proceeded thermal image preprocessing by following the steps below. As a result of the preprocessing, two thermal images with different contrast levels were created.

1. Input a raw image → *Figure 3.2* (b) Image A.
2. Adjust the image, *Figure 3.2* (b), to have a lower contrast level → *Figure 3.2* (a) Image A-L.
3. Adjust the image, *Figure 3.2* (b), to have a higher contrast level → *Figure 3.2* (c) Image A-H.

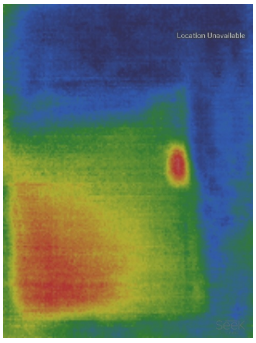

(a) Image A-L: Image (b) with low contrast level

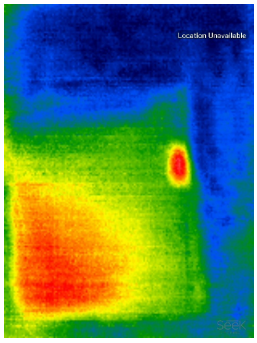

(b) Image A: Original frame

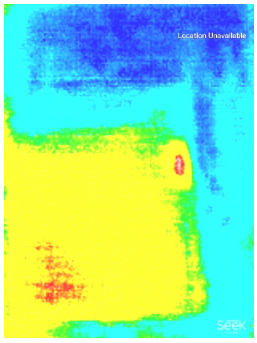

(c) Image A-H: Image (b) with high contrast level

Figure 3.2. Thermal image preprocessing

Appendix A.1 is an algorithm written in *Python* that used to adjust the contrast level of images. The key feature of the function is using *cv2.convertScaleAbs()* provided by *OpenCV*. The formula of the method is addressed in (3.1). The contrast level was adjusted by using α and β, respectively. α of 3 was used, and to lower the contrast level α of 0.5 was used to increase the contrast level.

i: pixel location of x,

j: pixel location of y,

$f(i,j)$: source image pixels,

$g(i,j)$: return image pixels,

α: optional scale factor for *Contrast*, and

β: optional scale factor for *Brightness*

$$g(i,j) = \alpha * f(i,j) + \beta \tag{3.1}$$

3.3 Fault Detection and Diagnosis

This research used a visual method of Fault Detection and Diagnosis (FDD) to inspect PV modules. FDD was realized by three algorithms written in *Python* using *OpenCV* library. The three FDD algorithms are: (i) fault detection, (ii) fault isolation, and (iii) fault identification. Throughout the FDD procedures, the hot spot phenomenon was identified, and the severity of each faulty area was measured. *Figure 3.3* is a flow chart of the FDD algorithms, and it gives an overview of each procedure. The details of the fault detection and diagnosis method are introduced in the following sections in this chapter.

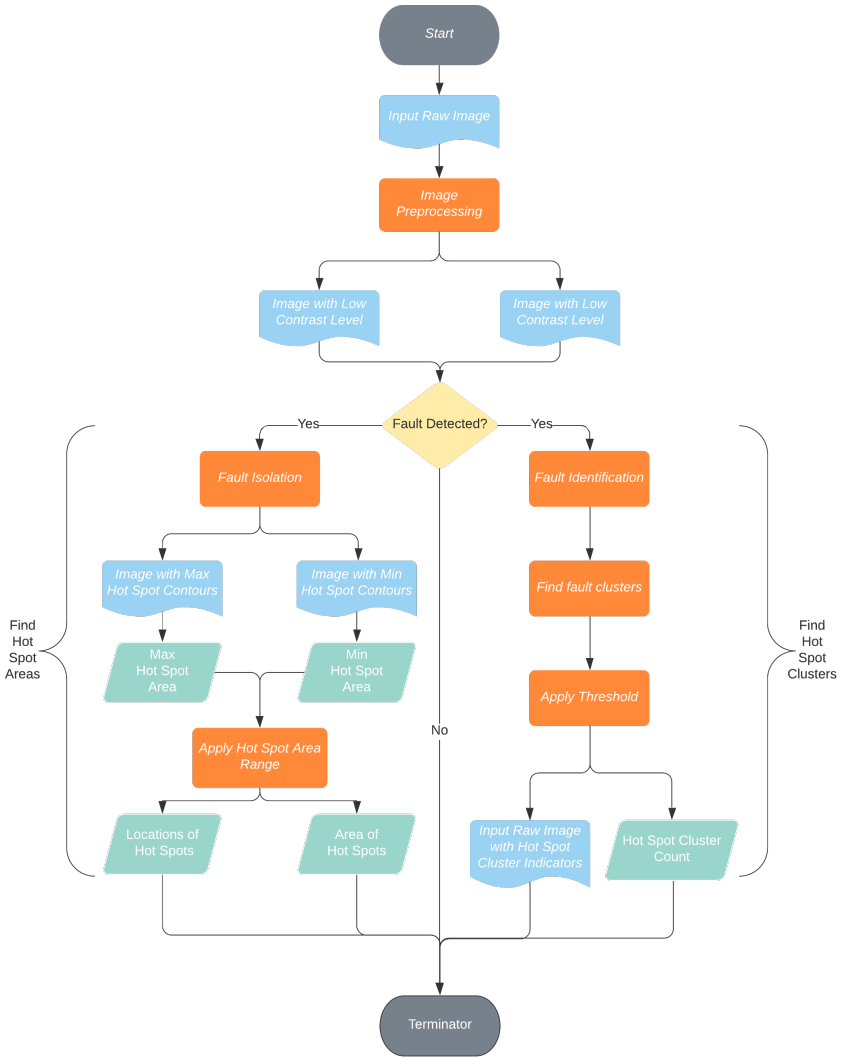

Figure 3.3. FDD algorithm flow chart

3.3.1 Fault Detection

Fault detection stage checks whether any abnormal condition was detected in the PV module or not. The abnormal conditions considered in this research are listed below.

- Unstable color representation in the PV module.
- Area that is colored in red (Hot Spot).
- Area that has higher ambient temperature than the surrounding area.

If no fault was found in this stage, the flow of the FDD model stops and the thermal image was sent to the next step, the fault isolation process.

3.3.2 Fault Isolation

The fault isolation stage starts if there was one of more fault(s) detected in the fault detection stage. In the fault isolation stage, the location and the size of PV faults were identified. If there was any hot spot detected, the exact location of them was measured as well as the size of them. In the fault isolation stage, all the faulty areas detected were taken into consideration for the next step.

Appendix A.2 is *faultIsolation()* function was built to find: (i) the area of PV fault and (ii) the original image with contour line indicators. *cv2.findContours()* is the key *OpenCV* method used in *faultIsolation()* function. This function was used to detect the red colored area(s) using upper and lower thresholds and highlight the area in the original thermal image. The detected areas were indicated by dark contour lines. The steps below summarize the fault isolation process.

1. Apply *faultIsolation()* on *Image A-L* $\rightarrow$ returns the max area of PV faults and the outer contours.
2. Apply *faultIsolation()* on *Image A-H* $\rightarrow$ returns the min area of PV faults and the inner contours.
3. Apply the outer and inner contours to the original image - *Image A*.

Figure 3.4 presents an example of how faulty areas were detected in the thermal images with different contrast levels. Possible faulty areas in both *Figure 3.2* (a) and *Figure 3.2* (c) were indicated with contour lines, as shown in *Figure 3.4* (a) and (c). The faulty area in *Figure 3.4* (a) being the maximum area of faults (the outer contour line in (b)) and the faulty area in *Figure 3.4* (c) being the minimum area of the faults (the inner contour line in (b)). Then the contours from both (a) and (c) were applied to the original image, *Figure 3.4* (b), to indicate the location of the PV faults range. In addition, the size of the contoured areas in *Figure 3.4* (a) and *Figure 3.4* (c) were calculated and returned as *maxArea* and *minArea*, respectively.

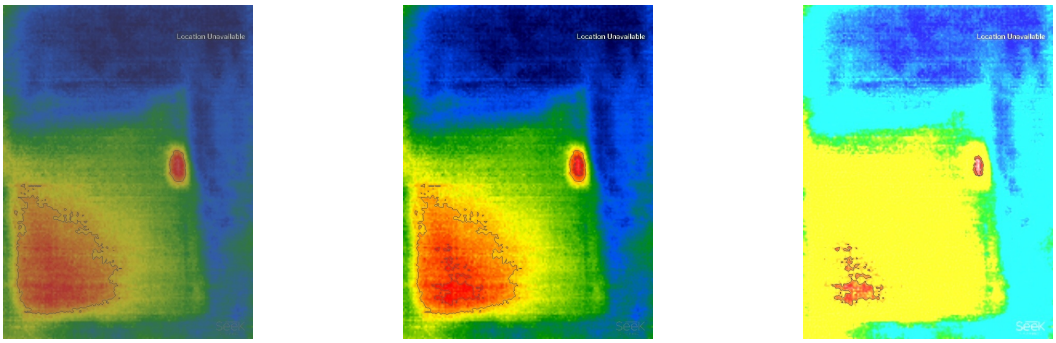

(a) Faulty area detected in *Image A-L*

(b) Faulty area range applied to *Image A*

(c) Faulty area detected in *Image A-H*

Figure 3.4. Faulty areas detected in different contrast levels

3.3.3 Fault Identification

In the fault identification stage, only the meaningful hot spot areas were identified using hot spot clustering. Based on the information achieved in the previous stage, the PV fault detection model found meaningful clusters of the hot spots isolated. *Figure 3.5* shows the final hot spots found in the model. First, it collected all hot areas possibly found in a thermal image, to create a pool. The pool of hot spot collection was in a grey-scale view, as presented in *Figure 3.5* (b). This pool might have some noise as well as the actual hot areas. Second, it found the hot spots by their size. A threshold was used to screen out only the meaningful hot areas in the hot spot pool. Appendix A.3 demonstrates the fault identification process.

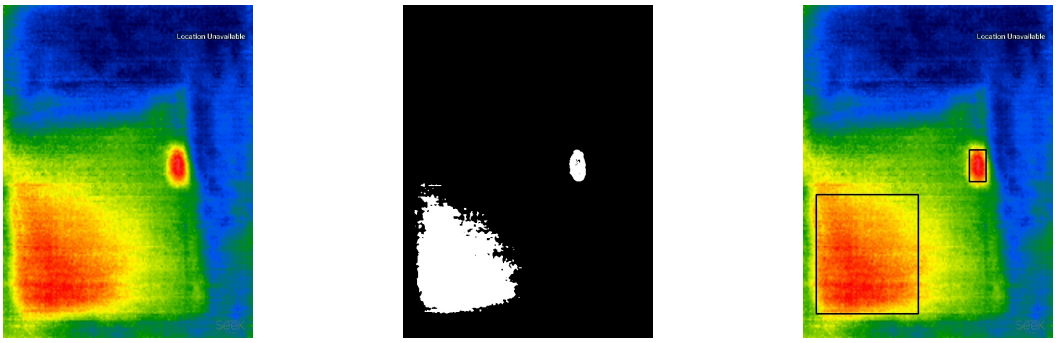

(a) Original image (b) Mask (c) Hot spot areas

Figure 3.5. Hot spot clusters identified

3.3.3.1 Noise filtering in fault identification

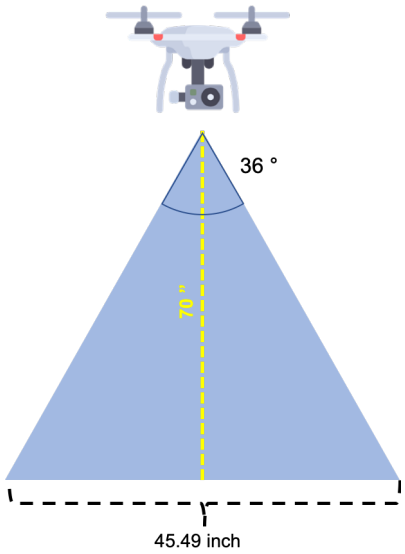

Figure 3.6. Camera distance and field of view

The used *Seek Thermal Compact camera* has a 36° field of view and resolution of 206x156 pixels. Measuring distance was set to 70 inches to gather close to the maximal amount of data from the PV module.

Image width from measuring distance of 70 inches:

$$2 * 70 * \tan 18^\circ = 45.49$$

The field of view at the widest direction of the camera view is 36 degrees. From a measuring distance of 70 inches from the PV module, the image captured is 45.49 inches wide. *Seek Thermal Compact camera* has 206 pixels to the widest direction of the image giving a pixel density to x-direction of 4.528 pixels per inch at the measuring distance of 70 inches.

Pixel density to x-direction at measuring distance of 70 inches:

$$\frac{206}{45.49} = 4.528 pixel/inch \tag{3.2}$$

Pixel density to both x-direction and y-direction from measuring distance of 70 inches:

$$4.528^2 = 20.50 pixel/sq.inch \tag{3.3}$$

The measured PV module had 36 (4 x 9) single solar cells sized 5 x 2.55 inches, each with an area of 12.75 *sq.inch*. Therefore, from a measuring distance of 70 inches, the captured images had on average of 261 pixels of data from each solar cell.

$$20.50 * 12.75 = 261.375 \approx 261 pixels \tag{3.4}$$

Thus, 250 pixels were selected as the minimum size for measured hot spots in the algorithm to ensure that individual solar cell faults would be detected, while smaller hot pixel noise caused by the camera's measurement inaccuracy was filtered out. The selected measurement distance could be further away, allowing the measurement of multiple PV modules at once with a more accurate thermal camera wingtra (n.d.).

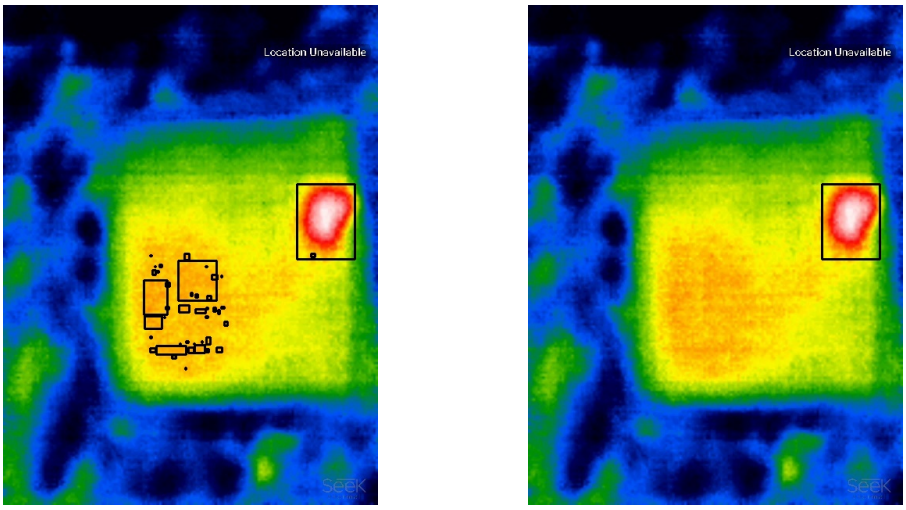

(a) With noise (b) Without noise

Figure 3.7. Filtering noises

3.4 Summary

Chapter 3 provided the thermal image analysis methodology on PV fault. It started with the introduction, followed by the thermal image data preprocessing method. Then it introduced the approach of the FDD. The data collection method and the analysis of the experiment result are addressed in the next chapter.

CHAPTER 4. RESULTS

4.1 Introduction

Chapter 4 deep dives into the experiment for data collection and the results of the experiment. The key feature of the experiment lies in aerial thermography. Cooperation of a UAV and a thermal camera can realize aerial thermography, which is a rising method for PV module inspection. Out of many PV faults that can be found during PV inspection, the research focuses on the hot spot phenomenon. Hot spot phenomenon appears on PV modules, and it is considered to be one of the crucial PV faults. Despite its severity, this phenomenon is not visible with naked eyes most times, as shown in *Figure 4.1*. This problem makes PV inspection more challenging. The research realized aerial thermography using a close-range UAV and a compact thermal camera for the data collection experiment, in order to overcome the challenges in hot spot capturing. The details of the experiment and the analysis of the result will follow in this chapter.

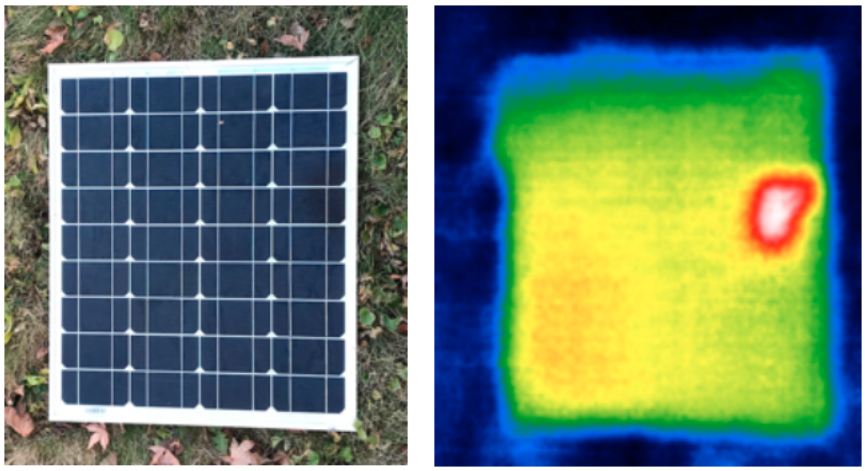

Figure 4.1. PV module with hot spot phenomenon

4.2 Experiment Setting

4.2.1 Hardware

Aerial Thermography (AT) was achieved by attaching a thermal sensor to a UAV. This study used a cost-efficient thermal camera compatible with *Android* devices. The thermal sensor, *Seek Thermal Compact (n.d.)*, was plugged into a micro USB port of the mobile device. Using a mobile device brings many benefits, such as network connectivity, lightweight, and access to both *Android* applications and computing power of the device. The thermal sensor plugged into the mobile device was mounted on the bottom of the UAV, *PHANTOM 2 (n.d.)*, to realize AT. The mounted thermal sensor collected thermal videos of a PV module. *Figure 4.2* shows how the thermal sensor, *Seek Thermal Compact (n.d.)*, was installed in the mobile device, *Acer Iconia 8 (n.d.)*, and *Figure 4.3* presents *PHANTOM 2 (n.d.)* with a mobile device mounted on the bottom of it.

Figure 4.2. Thermal camera, Seek Thermal Compact (n.d.), plugged into an Android device, Acer Iconia 8 (n.d.)

Figure 4.3. PHANTOM 2 (n.d.)

4.2.2 PV Module

The experiment chose to use a PV module that works in both sunny and overcast conditions and is fully weatherproof. A 12v 40w monocrystalline solar panel shown in *Figure 4.4* was used to collect thermal image data. This solar module has 36 PV cells (4 x 9) in itself and has a size of 631mm(w) x 554mm(h) x 30mm(d). Its best energy generation condition is known as more than 28ah per day, according to BSP (n.d.) The specifications of the PV module is present in Table 4.1. One important feature of the PV module used in this research is that it has a hot spot fault in itself, as shown in *Figure 4.1*.

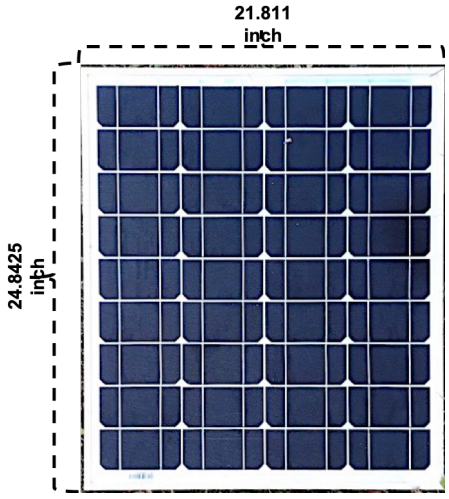

Figure 4.4. PV module size

Table 4.1. *PV module specifications*

Panel Size(w)	631mm
Panel Size(h)	554mm
Panel Size(d)	30mm
Weight	5.1kg
Open Circuit Voltage	21.5V
Short Circuit Current	2.64A
Max Power Voltage	17.5V
Max System Current	2.35A
Max System Voltage	300VDC
Number of Cells	36 (4 x 9)

The three different PV environments for data acquisition are: (a) no effect, (b) soiling effect, and (c) shading effect. Figure 4.5 describes how the three types of experiments were set up in the experiments. The experimental conditions were identical for all the experiments, but only the PV condition was set differently in each experiment. In *Figure 4.5* (a), the surface of the PV module was kept clean, and no obstacle or shade was on the panel. In *Figure 4.5* (b), dried maple leaves were used to realize the soiling effect. Lastly, in *Figure 4.5* (c), the shade effect was naturally made by the tree near the experiment site. The experiment with *Figure 4.5* (c) was done after the PV module was placed under the shade for about 45 minutes to have a full shading effect on the PV module.

(a) No effect (b) Soiling effect (c) Shading effect

Figure 4.5. Three different PV Conditions

4.3 Data Acquisition

All three experiments for data acquisition were conducted at an open area with the GPS coordinates of 40.425965,-86.909730 (DD) on the same day (November 26, 2019). The weather was sunny and windy. The temperature range during the experiment was between 50 ° F and 55 ° F. In this stage, video footage was collected instead of images due to image quality issues. When the thermal camera takes images while the UAV is flying, the images collected tend to have poor quality, as shown in *Figure 4.6* (a). To improve the quality of the data, the thermal image data was achieved through two steps: (i) collect thermal video data during the experiments, and (ii) extract thermal images from the collected videos using an *OpenCV (n.d.)* model. The thermal image present in *Figure 4.6* (b) is an example of the thermal frame extracted from a thermal video. This clearly shows the improvement between the two approaches for collecting data.

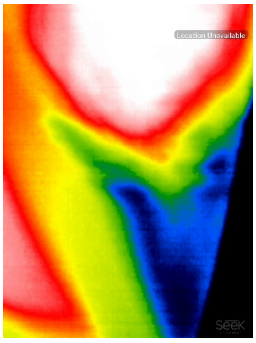

(a) Thermal image directly collected by aerial thermography

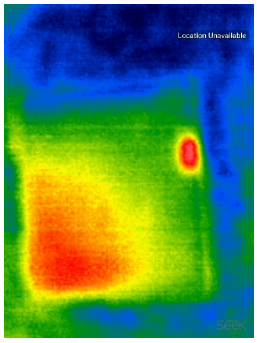

(b) Thermal image frame extracted from a thermal video

Figure 4.6. Difference in image quality

4.3.1 Aerial Thermography

Aerial thermography was realized by a close-range thermal UAV and a thermal camera sensor. The experiment design present in *Figure 4.7* describes the details of the close-range thermal UAV realization. The UAV was not flown by itself in the experiment, but it was used to mimic an actual UAV flying motion by being held from the pole. The T-shaped pole, shown in *Figure 4.7* (a), has a height of 120 inches, and the UAV was hanged by a string that was attached from the pole. The UAV was pulled and moved by an experimenter to mimic the UAV movement properly. *Figure 4.7* (b) describes how the UAV was moved during the experiment. Considering the size of the UAV and the PV module, the UAV did not need to move a big distance over the PV module. The motion of the close-range UAV realization was similar to a drone hovering over the PV module. This approach enabled data collecting much more stable, avoiding high errors. This method of using a UAV was referred by research done by Kim et al. (2019).

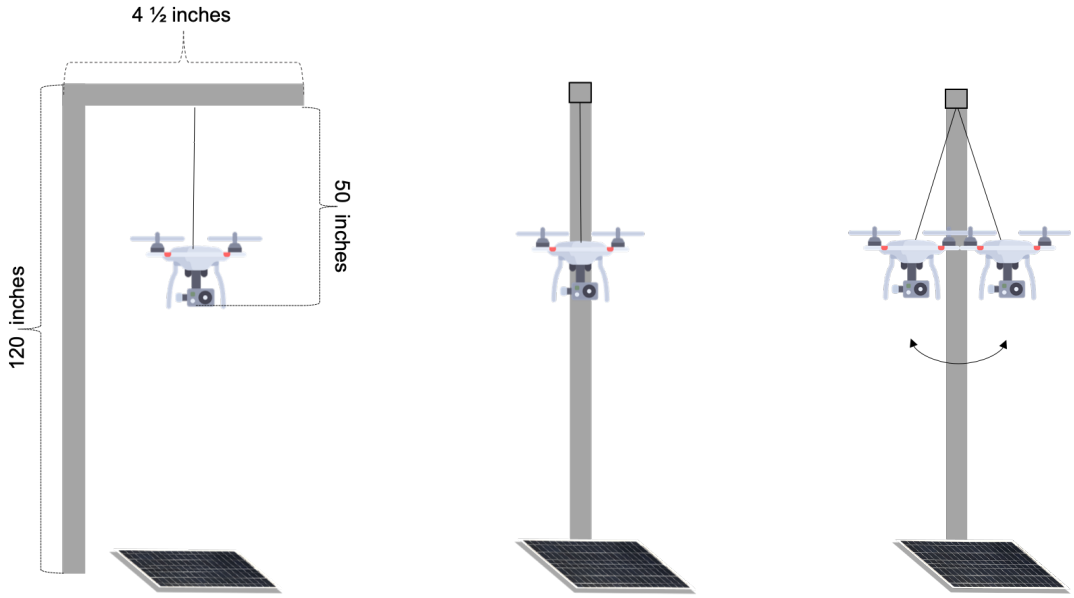

(a) Side view (b) Front view (c) Motion of the close-range UAV

Figure 4.7. Close-range thermal UAV realization. The UAV icon was made by Freepik (n.d.)

4.3.2 PV Monitoring

There were three types of PV monitoring experiments conducted in this research: (i) PV monitoring on a PV module with no effect, (ii) PV monitoring on a PV module with soiling effect, and (iii) PV monitoring on a PV module with shading effect. The thermal image data were collected during the three PV monitoring processes. The left experiment setup in *Figure 4.8*(a) was designed to collect the thermal video data of a PV module with no effect (*Figure 4.5* (a)). The experiment setup in *Figure 4.8*(b) was designed to collect the thermal video data of a PV module with the soiling effect (*Figure 4.5* (b)). Lastly, the right experiment setup in *Figure 4.8*(c) was designed to collect the thermal data of a PV module with the shading effect (*Figure 4.5* (c)).

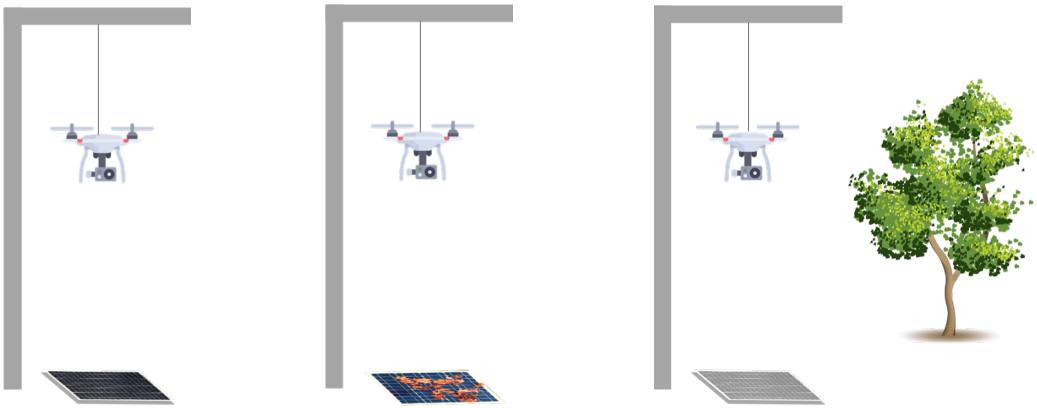

(a) No effect (b) Soiling effect (c) Shading effect

Figure 4.8. PV monitoring in the three different PV conditions. The UAV icon and the tree icon were made by Freepik (n.d.).

4.4 Experiment Result

4.4.1 Data collection result

A total of 15 thermal videos were successfully collected, and five videos were collected from each experiment type. The reason why more than one video was used for analysis is to collect a more significant number of videos for statistics. The metadata of the thermal videos collected in each experiment is introduced in Table 4.2. In the metadata, each length of the video data varied from 2 to 38 seconds. The data was collected to reflect the realistic data collection so that the video frames do not have the same duration. A short clip of video could generate more than enough image frames as long as the quality of the video is good. Therefore, the experimenter focused more on collecting good quality videos that could display the necessary features of the PV module than having all the videos meet the same length. Eventually, the average length of the collected thermal videos was about 18.5 seconds. For the video data collected, the research first extracted image frames from each video. The total frames count column in Table 4.2 shows the number of image frames that were extracted from each video. From this process, a total of 8349 thermal images were achieved.

However, not all the images were used in the image analysis because of their quality. The author looked through the image data and screened out only the good quality images that clearly present the PV module view in their frames. Frames used count column in Table 4.2 shows the number of frames used out of the total frames achieved from the collected videos. This concludes that out of 8349 frames, 5856 images were used in this research for thermal image analysis. Table 4.3 presents a summary of the data collection by each experiment type.

Table 4.2. *Data collection metadata*

Experiment Type	Take No.	Length (sec.)	Total frames (cnt.)	Frames used (cnt.)
No Effect	1	2	264	163
	2	12	356	283
	3	19	549	340
	4	25	728	652
	5	38	1112	725
Soiling Effect	6	12	365	258
	7	11	318	272
	8	15	363	322
	9	12	426	402
	10	22	648	516
Shading Effect	11	13	392	215
	12	22	650	538
	13	38	1136	336
	14	19	552	473
	15	17	490	361
Total Sum	15	277	8349	5856
Total Average	-	18.5	556.6	390.4

Table 4.3. *Summary of data collection by experiment types*

Experiment Type	No Effect	Soiling Effect	Shadow Effect
Avg. lengths (sec.)	19.2	14.4	21.8
Avg. total frame count	601.8	424	644
Avg. used frame count	432.6	354	384.6

4.4.2 Data analysis results

Since the research used one PV module with a fault in itself (*Figure 4.1*), there was no thermal image data identified as a non-faulty condition. *Figure 4.9* shows how the abnormal areas were found in each type of experiment.

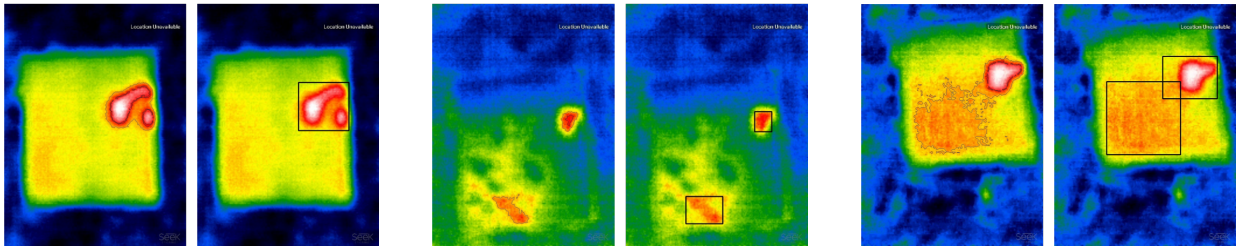

(a) Abnormal area found in a PV module with no effect

(b) Abnormal area found in a PV module with soiling effect

(c) Abnormal area found in a PV module with shading effect

Figure 4.9. Abnormal areas identified in all experiment

Thermal data analysis using the fault detection and diagnosis algorithm introduced in Chapter3 brought three types of information to this study: (i) minimum hot spot area in pixel (*minArea*), (ii) maximum hot spot area in pixel (*maxArea*) and (iii) the number of hot spots identified. The minimum hot spot area and the maximum hot spot area are used to estimate the range of the area size. Table 4.4 is the result of the data analysis. It has three types of information from the 15 thermal videos taken in the data collection stage. The samples of the thermal image data, collected and analyzed, are present in APPENDIX B.

Table 4.4. *Data analysis result*

Experiment Type	Take No.	minArea (pixel)	maxArea (pixel)	Hot spot (cnt.)
No Effect	1	1702.398773	18365.62883	0.938650307
	2	2791.869258	32877.18905	1.098939929
	3	2819.572059	32713.74706	1.391176471
	4	3391.222393	28170.14801	1.552147239
	5	3856.274483	19390.59655	1.227586207
Soiling Effect	6	4564.53876	32783.48062	2.209302326
	7	173.3014706	2208.134191	1.555147059
	8	8560.34472	50637.8944	1.760869565
	9	7255.731343	42995.48383	1.654228856
	10	544.6947674	8577.675388	2.36627907
Shading Effect	11	248.7744186	5433.474419	3.013953488
	12	881.4553903	11567.11524	1.678438662
	13	531.5431548	19916.93452	1.863095238
	14	233.2019027	7410.109937	2.687103594
	15	358.7714681	13945.08726	1.20498615
Average	15	2527.579624	21799.51329	1.746793611

Table 4.5 summarizes the hot spot areas calculated in the analysis stage. One noticeable thing is that the difference of the error ranges between the average minArea and the average maxArea is not significant for the no effect case and the soiling effect case. However, distinct differences in values are found in Avg. minArea data and Avg. maxArea data. Assuming that the experiment with no effect would only reflect the hot spot phenomenon, the data from the experiment with soiling effect tells bigger fault areas were detected than the no effect case. In the case of the shadow effect, the faulty areas detected were the least in both minAea and maxArea.

Table 4.5. *Fault area analysis by experiment types*

Experiment Type	Avg. minArea (pixel)	Avg. maxArea (pixel)	Error range (pixel)
No Effect	2912.267393	26303.4619	23391.19451
Soiling Effect	4219.722212	27440.53369	23220.81147
Shadow Effect	450.7492669	11654.54428	11203.79501

For a deeper understanding of the faulty area data, the author analyzed the weight of the fault detected over the PV module area. Having the knowledge of the number of PV cells, present in Table 4.1, and the number of pixels for each solar cell (3.4), it is possible to calculate the ratio of the PV module area affected by hot spots. The calculation below achieved that the estimated number of pixels in the image for the total solar cell area is 9409.5 pixels (4.1).

$$36 * 261.375 = 9409.5 pixels \tag{4.1}$$

The weight of the faults was measured by calculating the ratio of hot spot area over the area of the whole PV module. The equation (4.2) shows how the weight of the hot spot phenomenon in the PV module was calculated. In the equation, H is the area of the hot spot detected in the thermal images data, and P is the total solar cell area of the PV modules in pixel. Eventually, w indicates the area ratio of hot spot area over the PV module area.

$$w = \frac{H}{P} * 100(\%) \tag{4.2}$$

Table 4.6 shows the weights of the hot spots in each case of the experiment. The average weight indicates that the experiment with no effect case has about 31% of the hot spot area in the PV module while the soiling effect case has a higher value in weights and the shading effect case has a much lower value. The author interprets it as the thermal data of the soiling effect case had an impact from soiling obstacles. Since the weather on the experiment day was windy, the experimenter had to re-position the dry leaves to realize a soiling effect for each session of data collection. This is why the weights for the soiling effect case in Table 4.6 shows the high variance between the values. On the other hand, the shading effect case did not present the internal hot spot area precisely due to the ambient temperature difference created by the shade. For example, if the ambient temperature of the PV module is low, then the hot spot present in thermal views could be smaller than its actual size, and vice versa for the opposite situation. This explains why the weights for the shading weight case is not so significant, but the average weight value is small. Due to the weather and the temperature, the hot spot presentation on the thermal images were smaller than the ones in the no effect case. The cold ambient temperature made the PV module surface cooler. Also, the experiment for the shadow effect case was done in the last order so that the temperature of the experiment site became the lowest out of the three cases of the experiments.

Table 4.6. *Weight of faulty area*

Experiment Type	Take No.	Weight (%) (4.2)	Average Weight (%)
No Effect	1	18	31
	2	30	
	3	30	
	4	36	
	5	41	
Soiling Effect	6	49	45
	7	2	
	8	91	
	9	77	
	10	6	
Shading Effect	11	3	5
	12	9	
	13	6	
	14	2	
	15	4	

Lastly, the fault detection and diagnosis algorithm brought the number of hot spots detected in the thermal images. Table 4.7 presents the analysis of the hot spots count. The research used a PV module that has one hot spot area, as shown in the thermal view in Figure 4.1. With this regard, the correct answer for the hot spot count is one. The research calculated the error in the Avg. hot spot count in Table 4.7. The experiment with no effect case has 0 error. It can be interpreted that the hot spot areas shown in thermal images was just about the actual hot spot. In the case of the soiling effect, the error in the hot spot count was 1. The author interprets it as the error is due to the obstacles placed on the PV panel. The leaves on the PV module occurred ambient temperature differences and resulted in creating false hot spot areas in the thermal view. In the case of the shadow effect, the error of 1 was made because the shade created ambient temperature differences. The shades on the PV module created temporal hot and cold areas, and the FDD algorithm detected hot areas as hot spots.

Table 4.7. *Hot spot count analysis result by experiment types*

Experiment Type	Avg. Hot spot (cnt.)	Error in Hot spot (Rounded cnt.)
No Effect	1.241700031	0
Soiling Effect	1.909165375	1
Shadow Effect	2.089515426	1

CHAPTER 5. DISCUSSION AND CONCLUSIONS

5.1 Conclusions

The number of solar power installations is growing rapidly around the world in many different environments. Maintenance of these installations can be improved with the use of aerial thermography and accurate thermal IR image analysis. The research aimed to detect hot spot phenomenon exposed to no effect, soiling effect, and shading effect in a PV module. The suggested methods use aerial thermography and the FDD algorithm for PV inspection. The achieved results have shown the accuracy and reliability of the proposed methods to identify the hot spot phenomenon in the no effect PV condition. Nonetheless, the soiling and shading effects caused difficulties in accurate hot spot detection. Notably, the soiling on the PV module disturbed the hot spot presentation in thermal images. Additionally, the shading effect increases and also decreases the hot spot areas in thermal views because shade interrupts the ambient temperature. To conclude, this research is expected to contribute to the inspection of domestic applications of PV systems.

5.2 Discussion

Without any PV effects, the proposed thermal image analysis technique can contribute to identifying hot spot failures in detail. Furthermore, the present methods not only provide the size of the hot spot areas but also indicate the location and the number of hot spots. The contribution of this research for the modern methodology of PV inspection is in the detailed information on the hot spot phenomenon because it will help accurately diagnose the status of PV systems. Furthermore, the study proved that aerial thermography for PV inspection is cost-efficient while being an accurate method. On the other hand, by making a comparison of the PV conditions, the study noted that the performance of the thermal sensor must be taken into account in order to accurately detect hot spot phenomenon and PV conditions. Low quality thermal images are not sufficient in themselves to distinguish the PV conditions because the images capture soiling and shades as hot spots. For better accuracy, radiometric capability and sufficient accuracy are pre-requisites for conducting aerial thermography for PV inspection. However, high-performing sensors can enhance the accuracy of fault detection, but they can be costly for small-scale PV systems for domestic purposes. Therefore, the level of performance should be considered in terms of economic factors. For example, exploiting cutting-edge sensor technologies would still be worthwhile for large-scale PV installations such as utility-scale solar power plants, while the FDD method introduced in this study should be enough for domestic PV installations.

Related literature supports the findings and conclusions of this study. Aghaei, Gandelli, Grimaccia, Leva, and Zich (2015) found out that aerial thermography can detect hot spots in optimal conditions. However, their study did not attempt to detect hot spots with shading or soiling effect. Jiang, Su, and Li (2016) also noted that shading effects would significantly increase the noise in thermal images and hot spot detection is reliable in optimal conditions because “the thermal images suffer from relatively high stochastic noise and non-uniformity clutter caused by the complex environment and emissivity uncertainty” (p. 4). Notably, Jiang et al. (2016) tried to overcome the noise on PV modules generated from dust or internal faults by applying curve fitting of gray histogram. Márquez and Ramírez (2019) studied the efficiency of aerial thermography by detecting soiling effects on solar panel installations. They were able to detect soiling effects reliably by using a radiometric thermal camera in combination with a UAV.

5.3 Limitations

The thermal camera used in this study was of a lower quality, which reduces the amount of valuable information gathered greatly. Also, due to the inaccuracy of the used thermal camera, the drone could not be actually flown and was instead hung from a string at a close distance to the PV module, so that sufficient quality images could be gathered. Even with these limitations, aerial thermography was shown to be able to detect hot spots in a PV module. However, for practical utilization of the method, a thermal camera with better accuracy, higher resolution, and radiometric capability is necessary (Gallardo-Saavedra et al., 2018). This will allow thermal imaging from greater distances with better quality.

5.4 Future work

To continue this research, improvements in the used methodology are necessary. A combination of a thermal camera with radiometric capability and a visual spectrum camera could lead to better ability to distinguish the soiling effect and shading effects. To improve the image recognition algorithm, a neural network could be used to improve the image recognition algorithm with a sufficiently large amount of training data that could be gathered. Lastly, an optimization of the flight paths during an inspection could be applied to future methods.

REFERENCES

Acer Iconia 8. (n.d.). (Available online: https://www.acer.com/ac/en/US/content/series/iconiaone8)

Aghaei, M., Gandelli, A., Grimaccia, F., Leva, S., & Zich, R. (2015). Ir real-time analyses for pv system monitoring by digital image processing techniques. In *2015 international conference on event-based control, communication, and signal processing (ebccsp)* (pp. 1–6).

Allinson, D. (2007). *Evaluation of aerial thermography to discriminate loft insulation in residential housing*. University of Nottingham.

Becker, S. (2019a, February). *The ultimate guide to community solar.* SOLSTICE. (Retrieved from https://solstice.us/solstice-blog/ultimate-guide-community-solar/)

Becker, S. (2019b, March). *A look into america's largest solar farm.* SOLSTICE. (Retrieved from https://solstice.us/solstice-blog/a-look-into-americas-largest-solar-farm/#targetText=Solar\20Star\2C\20America's\20largest\20solar\20farm\2C\20was\20actually\20the\20biggest,and\20Los\20Angeles\20Counties\2C\20California)

BSP. (n.d.). *12v 40w monocrystalline solar panel rigid.* (Retrieved from ttp://www.bsp.lt/en/12v-sauls-elementai/28-12v-40w-monocrystalline-solar-panel-rigid.tml)

Cano, J. (2011). *Photovoltaic modules: Effect of tilt angle on soiling*. Arizona State University.

Constantin, A., & Dinculescu, R.-N. (2019). Uav development and impact in the power system. In *2019 8th international conference on modern power systems (mps)* (pp. 1–5).

Cubukcu, M., & Akanalci, A. (2020). Real-time inspection and determination methods of faults on photovoltaic power systems by thermal imaging in turkey. *Renewable Energy*, *147*, 1231–1238.

Deng, Z. Z. J. C. D. J. X. Z. Y. X. X. T., S., & Xing, G. (2017). Research on hot spot risk for high-efficiency solar module. *Energy Procedia*, *130*, 77-86.

Denio, H. (2012). Aerial solar thermography and condition monitoring of photovoltaic systems. In *2012 38th ieee photovoltaic specialists conference* (pp. 000613–000618).

Deutsche Gesellschaft für Sonnenenergie (DGS). (2013). *Planning and installing photovoltaic systems: a guide for installers, architects and engineers*. Routledge.

Ellsmoor, J. (2019, June). *Renewable energy is now the cheapest option - even without subsidies.* Forbes. (Retrieved from https://www.forbes.com/sites/jamesellsmoor/2019/06/15/renewable-energy-is-now-the-cheapest-option-even-without-subsidies/#60484a975a6b)

Fagnani, R. (2016, October). *Solar asset management.* (Retrieved November 1, 2019 from https://europe.solar-asset.management/new-updates-source/2016/10/31/the-pv-modules-soiling-issue-our-final-solutions)

Farret, F. A., & Simões, M. G. (2017). *Integration of renewable sources of energy*. John Wiley & Sons.

FLIR. (2019, July). *A guide to inspecting solar fields with thermal imaging drones.* (Retrieved from https://thermalcapture.com/wp-content/uploads/2019/08/pv-system-inspection-thermal-drones-07-15-19.pdf)

Fluke. (n.d.). What is infrared thermography?

(Retrieved November 1, 2019, from https://www.fluke.com/en-us/learn/best-practices/measurement-basics/thermography/what-is-infrared-thermography)

Fraunhofer Institute for Solar Energy Systems,
I. w. s. o. P. G. (2019, November). *Photovoltaics report.* (Retrieved from ttps://www.ise.fraunofer.de/content/dam/ise/de/documents/publications/studies/Photovoltaics-Report.pdf)

Freepik. (n.d.). (Icon made by Freepik from http://www.freepik.com)

Gallardo-Saavedra, S., Hernández-Callejo, L., & Duque-Perez, O. (2018). Technological review of the instrumentation used in aerial thermographic inspection of photovoltaic plants. *Renewable and Sustainable Energy Reviews*, *93*, 566–579.

George, P. (2014, July). *Bp says the world only has 53 years of oil left, should you panic?* Jalopnik. (Retrieved from https://jalopnik.com/its-v12-time-1839549612)

Gertler, J. (2017). *Fault detection and diagnosis in engineering systems*. Routledge.

Glavaš, H., Vukobratović, M., Primorac, M., & Muštran, D. (2017). Infrared thermography in inspection of photovoltaic panels. In *2017 international conference on smart systems and technologies (sst)* (pp. 63–68).

Google Scholar. (n.d.). *About.* (Retrieved November 1, 2019, from https://scholar.google.com/intl/en/scholar/about.html)

Hernández-Callejo, L., Gallardo-Saavedra, S., & Alonso-Gómez, V. (2019). A review of photovoltaic systems: Design, operation and maintenance. *Solar Energy*, *188*, 426–440.

Hodge, T. (2019, January). *Eia forecasts renewables will be fastest growing source of electricity generation.* U.S. Energy Information Administration. (Retrieved from https://www.eia.gov/todayinenergy/detail.php?id=38053)

IEA. (n.d.). Renewables 2019.

(Retrieved October 31, 2019, from https://www.iea.org/renewables2019/#targetText=Renewables\202019\20is\20the\20IEA,electricity\2C\20heat\20and\20transport\20sectors)

IEEE Xplore® Digital Library. (n.d.). *About ieee xplore® digital library.* (Retrieved November 1, 2019, from https://ieeexplore.ieee.org/xpl/aboutUs.jsp#targetText=The\20IEEE\20Xplore\20digital\20library,Engineers)\20and\20its\20publishing\20partners)

Jaffery, Z. A., Dubey, A. K., Haque, A., et al. (2017). Scheme for predictive fault diagnosis in photo-voltaic modules using thermal imaging. *Infrared Physics & Technology*, *83*, 182–187.

Jean-Paul, R., & Claude, C. (2017). The environmental impacts of transportation. *The Geography of Transport Systems, New York, Routledge*.

Jiang, L., Su, J., & Li, X. (2016). Hot spots detection of operating pv arrays through ir thermal image using method based on curve fitting of gray histogram. In *Matec web of conferences* (Vol. 61, p. 06017).

Kauppinen, T., Panouillot, P.-E., Siikanen, S., Athanasakou, E., Baltas, P., & Nikopoulous, B. (2015). About infrared scanning of photovoltaic solar plant. In *Thermosense: Thermal infrared applications xxxvii* (Vol. 9485, p. 948517).

Kim, K., Choi, Y., Shim, K., Jeon, H., Commerford, J., & Matson, E. T. (2019). Analyzing the range of angles of a solar panel to detect defective cells, using a uav. In *2019 third ieee international conference on robotic computing (irc)* (pp. 471–476).

Lee, D., & Park, J. (2019). Developing inspection methodology of solar energy plants by thermal infrared sensor on board unmanned aerial vehicles. *Energies*, *12*(15), 2928. (Retrieved from https://www.mdpi.com/1996-1073/12/15/2928)

Lynn, P. A. (2011). *Electricity from sunlight: an introduction to photovoltaics*. John Wiley & Sons.

Maghami, M. R., Hizam, H., Gomes, C., Radzi, M. A., Rezadad, M. I., & Hajighorbani, S. (2016). Power loss due to soiling on solar panel: A review. *Renewable and Sustainable Energy Reviews*, *59*, 1307–1316.

Mapundu, S. (2018). Thermography based fault detection and diagnosis in photovoltaic systems using drones.

Márquez, F. P. G., & Ramírez, I. S. (2019). Condition monitoring system for solar power plants with radiometric and thermographic sensors embedded in unmanned aerial vehicles. *Measurement*, *139*, 152–162.

MATASCI, S. (2019, July). *How much do solar panels cost in the u.s. in 2019?* (Retrieved from `https://news.energysage.com/how-much-does-the-average-solar-panel-installation-cost-in-the-u-s/`)

Mellit, A., Tina, G. M., & Kalogirou, S. A. (2018). Fault detection and diagnosis methods for photovoltaic systems: A review. *Renewable and Sustainable Energy Reviews*, *91*, 1–17.

Molenbroek, E., Waddington, D., & Emery, K. (1991). Hot spot susceptibility and testing of pv modules. In *The conference record of the twenty-second ieee photovoltaic specialists conference-1991* (pp. 547–552).

Olalla, C., Hasan, M., Deline, C., & Maksimović, D. (2018). Mitigation of hot-spots in photovoltaic systems using distributed power electronics. *Energies*, *11*(4), 726.

OpenCV. (n.d.). (Available online: `https://opencv.org/`)

Parida, B., Iniyan, S., & Goic, R. (2011). A review of solar photovoltaic technologies. *Renewable and sustainable energy reviews*, *15*(3), 1625–1636.

PHANTOM 2. (n.d.). (Available online: `https://www.dji.com/phantom-2`)

Piliougine, M., Carretero, J., Mora-López, L., & Sidrach-de Cardona, M. (2011). Experimental system for current–voltage curve measurement of photovoltaic modules under outdoor conditions. *Progress in photovoltaics: research and applications*, *19*(5), 591–602.

Piliougine, M., Carretero, J., Sidrach-de Cardona, M., Montiel, D., & Sánchez-Friera, P. (2008). Comparative analysis of the dust losses in photovoltaic modules with different cover glasses. In *Proceedings of 23rd european solar energy conference, valencia, spain* (pp. 2698–2700).

Portland Cement Association. (n.d.). *Thermal anomaly.* (Retrieved November 1, 2019, from https://www.cement.org/buildingcodes/structural-design/energy-performance/thermal-anomaly)

Renewable Energy World. (2019, April). *What is a solar farm?* (Retrieved from https://www.renewableenergyworld.com/2019/04/30/what-is-a-solar-farm/#gref)

Samlex America Inc. (n.d.). Pv cell, module, array. (Retrieved November 1, 2019 from https://www.samlexsolar.com/learning-center/solar-cell-module-array.aspx)

ScienceDirect. (n.d.). (Retrieved November 1, 2019, from https://www.sciencedirect.com/)

Seek Thermal Compact. (n.d.). (Available online: https://www.thermal.com/compact-series.html)

Solar Review. (2018, October). *Solar panel hot spot (tier-1) exposed!* (Retrieved from https://review.solar/solar-panel-hot-spot/)

Springer. (n.d.). *About about springer.* (Retrieved November 1, 2019, from https://www.springer.com/gp/about-springer)

Stridh, B. (2012). Evaluation of economical benefit of cleaning of soiling and snow in pv plants at three european locations. In *2012 38th ieee photovoltaic specialists conference* (pp. 001448–001451).

SunPower. (n.d.). A complete guide to 7 renewable energy sources. (Retrieved November 1, 2019, from https://us.sunpower.com/complete-guide-7-renewable-energy-sources)

the U.S. Energy Information Administration. (2019, September). *How much oil is consumed in the united states?* (Retrieved from https://www.eia.gov/tools/faqs/faq.php?id=33&t=6)

UgCS. (n.d.). *Pv solar panel field inspection with ugcs.* (Retrieved October 31, 2019, from https://www.ugcs.com/page/solar-panel-inspection-with-ugcs)

United States Department of Labor. (n.d.). Green job hazards: Solar energy. occupational safety and health administration. (Retrieved October 31, 2019, from https://www.osha.gov/dep/greenjobs/solar.html#targetText=Workers\20in\20the\20solar\20energy,can\20cause\20injury\20and\20death)

U.S. Department of Energy. (2018). *Solar energy technologies office.* SOLAR ENERGY TECHNOLOGIES OFFICE. (Retrieved from https://www.energy.gov/sites/prod/files/2018/02/f48/2018\20SETO\20Portfolio\20Book.pdf)

Willoughby, J. (2019, October). *Drones for solar panel inspections.* (Retrieved from https://www.heliguy.com/blog/2019/10/24/drones-for-solar-panel-inspections/)

wingtra. (n.d.). *How ground sample distance (gsd) relates to accuracy and drone roi.* (Retrieved from ttps://wingtra.com/ow-ground-sample-distance-gsd-relates-to-accuracy-and-drone-roi)

APPENDIX A. PV FAULT DETECTION AND DIAGNOSIS ALGORITHMS

```
    def adjustContrast(self, img, alpha):
        beta = 50  # Brightness control (0-100)

        # Adjusting contrast
        return cv2.convertScaleAbs(img, alpha=alpha, beta=beta)
```

Listing A.1: Image Preprocessing Model

```
    def faultIsolation(self, img, opt):
        if img is None:
            return None, None

        image = img.copy()
        hsv = cv2.cvtColor(image, cv2.COLOR_BGR2HSV)

        # Fault range
        con = Contour(opt)
        lower = np.array(con.LOWER_THRESHOLD, dtype="uint8")
        upper = np.array(con.UPPER_THRESHOLD, dtype="uint8")

        mask = cv2.inRange(hsv, lower, upper)

        cnts = cv2.findContours(mask, cv2.RETR_EXTERNAL,
                                cv2.CHAIN_APPROX_SIMPLE)
        cnts = cnts[0] if len(cnts) == 2 else cnts[1]

        area = 0
        for c in cnts:
            # sum all areas
            area += cv2.contourArea(c)
            cv2.drawContours(self.raw, [c], 0, con.COLOR, 1, cv2.LINE_8)

        contour = self.raw.copy()
```

```
26
27          return area, contour
```

Listing A.2: Fault Isolation Model

```
1   def faultIdentification(self):
2       if self.raw is None:
3           return None, None, None
4
5       image = self.raw.copy()
6       hsv = cv2.cvtColor(image, cv2.COLOR_BGR2HSV)
7
8       # Fault range
9       lower = np.array(Contour('OUTER').LOWER_THRESHOLD, dtype="uint8")
10      upper = np.array(Contour('OUTER').UPPER_THRESHOLD, dtype="uint8")
11
12      mask = cv2.inRange(hsv, lower, upper)
13
14      ret, thresh = cv2.threshold(mask, 250, 255, 0)
15
16      # Finding clusters
17      n_labels, labels, stats, centroids
18                              = cv2.connectedComponentsWithStats(thresh)
19      total_cnt = n_labels - 1
20      cnt = 0
21      size_thresh = 1
22
23      for i in range(1, n_labels):
24          if stats[i, cv2.CC_STAT_AREA] >= size_thresh:
25              x = stats[i, cv2.CC_STAT_LEFT]
26              y = stats[i, cv2.CC_STAT_TOP]
27              w = stats[i, cv2.CC_STAT_WIDTH]
28              h = stats[i, cv2.CC_STAT_HEIGHT]
29              a = stats[i, cv2.CC_STAT_AREA]
30
31              if 250 < a:
32                  cnt += 1
```

```
                    cv2.rectangle(image, (x, y), (x + w, y + h),
                                                  (0, 0, 0), thickness=2)

        return total_cnt, cnt, image
```

Listing A.3: Fault Identification Model

APPENDIX B. THERMAL DATA COLLECTED AND ANALYSED

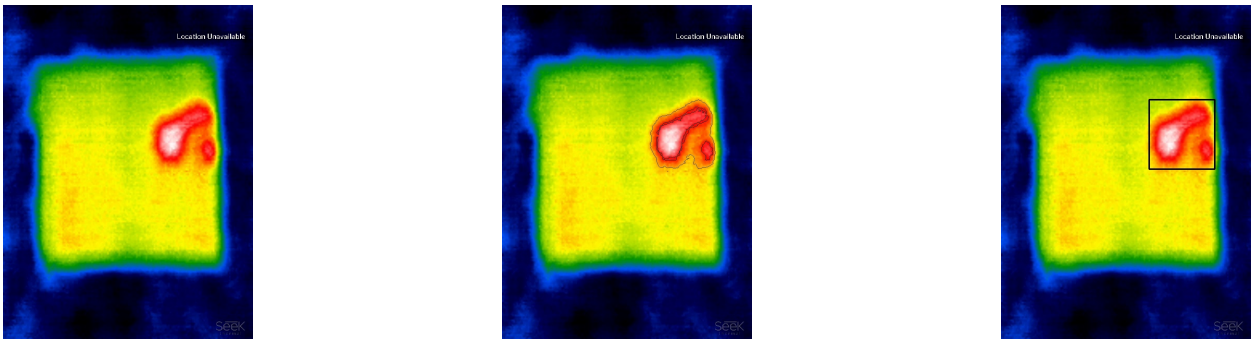

Figure B.1. Thermal Data from Experiment (i) No effect

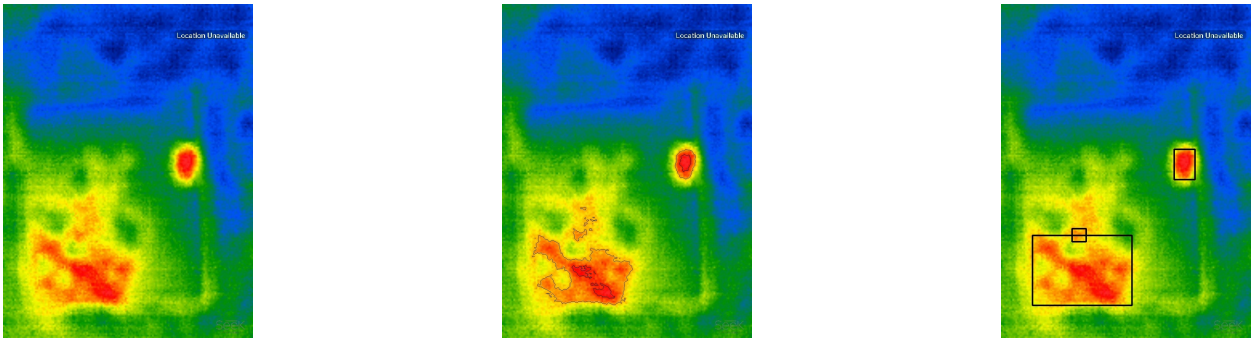

Figure B.2. Thermal Data from Experiment (ii) Soiling effect

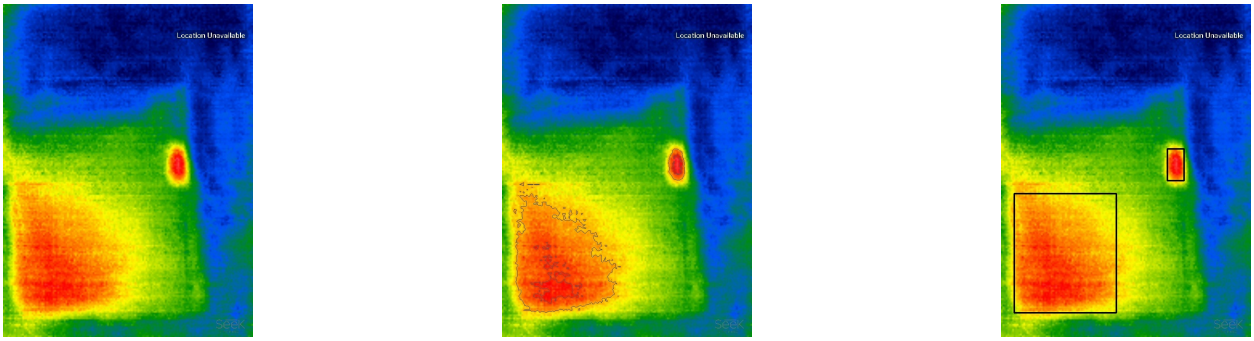

Figure B.3. Thermal Data from Experiment (iii) Shading effect